PROCEEDINGS, 42nd Workshop on Geothermal Reservoir Engineering
Stanford University, Stanford, California, February 13-15, 2017
SGP-TR-212

Probabilistically Assessing the Efficacy of Stimulation Strategies

Dimitrios Karvounis and Stefan Wiemer

Swiss Seismological Service, ETH Zurich, Sonneggstrasse 5, 8092 Zurich, Switzerland

karvounis@sed.ethz.ch

Keywords: EGS, induced seismicity, modeling, PSHA

ABSTRACT

According to the energy strategy of Switzerland for the year 2050, deep geothermal technologies like Enhanced Geothermal Systems (EGS) need to provide approximately 7% of Switzerland's electricity supply. In order for this strategic goal to be reached, not only further fundamental and applied researches are required, but also several stakeholders such as the investors, the local community and the regulatory authorities should harmoniously collaborate. Important decisions that are related to induced seismicity, need to be made at periods of high uncertainty and need to be as mutually acceptable as possible.

Computational tools are currently developed by the Swiss Seismological Service (SED) that integrate over the space of this uncertainty and aim to return forecasts of the efficacy of a stimulation strategy for a number of different criteria. Probabilistic long term forecasts of EGS operations are obtained by performing Monte Carlo simulations both for the creation and the production phase. The former is important for probabilistically assessing the induced seismicity hazard (e.g. in a real-time traffic light application) and the latter for assessing the commerciality of a stimulation strategy. Each realization of the Monte Carlo simulation considers a different but still probable sequence of induced seismicity events that has been sampled according to observed statistical field observations and to how pore-pressure is expected to have evolved for the modeled sequence of events. Pore-pressure and temperature propagations are modeled with HFR-Sim, which is the in-house EGS simulator that employs a 3D embedded discrete fracture model for modeling flow and heat transport inside an EGS reservoir. HFR-Sim has been especially designed for such dynamically changing fracture networks, it can simulate a wide range of probable EGS scenarios in reasonable return times, and the hydraulic effect of many induced seismicity related field observations can be quickly approximated. Here, we focus on numerical recipes and simplifications that significantly prolong the forecasting ability. An exemplary Monte Carlo simulation is presented and discussed.

1. INTRODUCTION

According to the Energy Strategy 2050 realized by the Swiss Federal Office of Energy, deep geothermal technologies are expected to grow enough for providing approximately 7% of Switzerland's electricity needs by the year 2050. Switzerland will gradually phase-out nuclear technology, which currently is responsible for 41% of Swiss power generation, and deep geothermal technologies like Enhanced Geothermal Systems (EGS) will cover a portion of the energy supply from nuclear power plants that has to be replaced. For that goal to be achieved, tens of EGS power plants need to be developed in the forthcoming decades. Challenges ahead do not include only the minimization of all costs related to EGS technology, but also social acceptance and the governance of the induced seismicity risk (Trutnevyte and Wiemer, 2017).

We focus here on forecasting the outcomes from two important phases in the lifetime of an EGS power plant; the 'creation phase' and the 'production phase'. The creation phase includes the stimulation of all the wells that are drilled for an EGS power plant and it precedes the production phase. During the creation phase, large rates of fluid are injected according to a stimulation strategy (F_{inj}) and seismicity is induced mostly due to the so-called process of "hydro-shearing". After a successful creation phase, the power required by the pumps for circulating fluids is significantly less and thus, geothermal heat can be extracted at commercially interesting rates and without causing large overpressures that can reactivate fractures. During the production phase the geothermal energy that has been stored in the reservoir of the EGS is extracted by circulating fluids through the stimulated wells. A portion of the extracted energy can then be converted to electrical energy and the remaining heat from the conversion cycle can be used for district heating or for other applications that require warm water. Electrical power generation continues for as long as hot enough fluids are produced and thermal breakthrough is avoided. The life expectancy of the EGS power plant strongly depends on the properties of the deformed fracture network and affects the commercial success of an EGS project.

A successful EGS power plant cannot be achieved unless a successful creation phase has preceded the production phase. EGS operators need to decide the injection strategy F_{inj} and modify it during stimulation. Thanks to a properly chosen strategy not only the induced seismicity hazard is low at all times and acceptable by the local regulatory authorities, but also the commercial success of the EGS power plant is guaranteed. Such criteria can be contradicting however. The induced seismicity hazard in general increases as the total injected volume increases, but then the commercial success of an EGS project can be less likely. The ability to forecast both of the induced seismicity during the creation phase and of the amount of energy that is produced in the subsequent production phase are desired, since then, the efficacy of different stimulation strategies can be quantitatively assessed, optimal well operations can be found, and the resolution of conflicts between the various stakeholders of the project can be accelerated.

Forecasting induced seismicity, which by itself is not a trivial task, is a necessary step for forecasting the subsequent production phase. Different methods for forecasting induced seismicity as well as an overview of unresolved challenges are reviewed by Gaucher et al.

(2015). The forecasting abilities and the complexity of the various models that forecast induced seismicity for a given scenario vary a lot. Recently, Király-Proag et al. (2016) studied methods for validating forecasts against observed seismicity in a real-time framework and showed how ensemble forecasting can be performed, where different forecasts are combined in a new and superior forecast. Real-time validation of the forecasts from various induced seismicity models is important for the development of sophisticated traffic light models (Karvounis et al., 2014).

Single EGS simulations have limited forecasting abilities when it comes to induced seismicity. EGS simulators return a unique approximation of the solution of an analytical model. However, such deterministic forecasts are representative enough of the real scenario, only when the analytical model is valid and all of its parameters are well defined. Especially during the early phases of an EGS project (i.e. beginning of the creation phase) this amount of information is not feasible. Thus, forecasts of the creation phase and estimations of the induced seismicity hazard can be only probabilistic. For the same reasons, forecasts of the production phase for a stimulation strategy F_{inj} have to be probabilistic too.

Here we focus on the further development of the framework of the hybrid model that employs the EGS simulator HFR-Sim, which simulator returns deterministic and realistic forecasts of the pore pressure propagation inside an EGS reservoir. With this hybrid model Monte Carlo (MC) integration over the space of uncertainty is performed in order to obtain probabilistic forecasts. It is done so by sampling a large number of equally probable geological models and probable hypocenters, then each model is simulated for the under-study scenario, and the probability of a certain outcome is approximated by the frequency with which these outcomes are presented in the simulations.

2. GOVERNING EQUATIONS OF THE HYBRID MODEL

Here, the hybrid model that is described in Karvounis and Wiemer (2015) is considered. It combines deterministic 3D discrete fracture modeling for flow and heat transport with stochastic modeling for the location, the time source and the magnitude of induced seismicity events. The deterministic modeling is performed with HFR-Sim and the stochastic modeling is performed with the so-called 'seed model', variations of which have been employed by many hybrid models in the past (Goertz-Allmann et al., 2011, Gischig et al., 2014, Catalli et al., 2016, Rinaldi and Nespoli, 2016).

2.1 Deterministic modeling

Henceforth, single phase laminar flow of a fluid that has constant dynamic viscosity μ and constant fluid's density ρ are assumed everywhere inside the domain Ω, which Ω represents the reservoir of an EGS. Gravitational effects are also neglected. Mass balance inside Ω can be expressed as

$$\frac{\partial \varphi}{\partial p}\frac{\partial p}{\partial t} + \nabla \cdot \left(\underbrace{-\frac{\boldsymbol{K}}{\mu} \cdot \nabla p}_{\vec{u}} \right) = q \,, \tag{1}$$

where φ is porosity, p is the fluid's pore-pressure, $\boldsymbol{K}$ is the permeability tensor, and q is a volumetric source term that includes the injection and production rate as well as the exchange rate through the far field boundaries of Ω. The specific discharge of the fluid inside the discrete fractures and the medium that surrounds the fractures is the term $\vec{u}$ and is a vector. A linear relationship is assumed between porosity and pore-pressure, according to which, porosity increases linearly with pore-pressure. When seismicity is absent, eq. (1) is considered linear and neither porosity nor permeability change. However, they increase instantaneously along the slipped surface when seismicity occurs. Deterministic solutions of eq. (1) are required both for simulating the creation phase and the production phase.

For simulating the production phase, the equations of energy conservation need to be satisfied besides mass conservation in eq. (1). Inside the fractures, heat advection is considered the dominating heat transport mechanism, contrary to the solid medium that surrounds the fractures. Inside the solid medium, conduction is the dominating mechanism. Conservation of energy inside the fluid and inside the solid medium are respectively expressed as

$$\frac{\partial \varphi \rho \boldsymbol{h}}{\partial t} + \nabla \cdot \left(\rho \boldsymbol{h} \vec{u} \right) = \dot{w} + \dot{w}_w + \dot{w}^r \,, \tag{2}$$

and

$$\frac{\partial (1-\varphi)\rho^r h^r}{\partial t} - \nabla \cdot \left(\boldsymbol{\Lambda} \nabla T^r \right) = \dot{w}_s - \dot{w}^r \,, \tag{3}$$

where h is the specific enthalpy of the fluid, $\dot{w}$ is the heat exchanged with the far field boundaries of Ω, $\dot{w}_w$ is a source term that quantifies the heat exchange rate through the well or wells, $\dot{w}^r$ is the heat flux from the solid phase to the fluid inside Ω, ρ^r is the density of the solid materials, h^r its specific enthalpy, $\boldsymbol{\Lambda}$ the heat conductivity tensor, T^r the temperature of the solid and $\dot{w}_s$ is a heat source term. The heat exchange between the fluid and the solid phase is proportional to the temperature difference between them; i.e. $\dot{w}^r = c(T^r - T)$, where c is a heat exchange coefficient.

The total thermal energy E_{th} that is produced from over a period of time t_l is

$$E_{th} = -\int_0^{t_l} \left(\int_\Omega \dot{w}_w d\Omega \right) dt \,. \tag{4}$$

Note that only a portion of the total thermal energy extracted can be converted to electrical energy. When the efficiency of this conversion is known, then the size of the electrical power production can be estimated.

2.2 Stochastic geomechanical modeling

Necessary condition for a fracture to be reactivated is the shear stress τ along the fracture to be over the frictional strength of the fracture. Due to high pore pressure, an induced seismicity event with hypocenter $\vec{x}_s$ and source time t_s is expected if the Mohr-Coulomb failure criterion is satisfied such that

$$p(\vec{x}_s, t_s) \geq \sigma_n + \frac{C_0 - \tau}{\mu_s} \,, \tag{5}$$

where σ_n is the component of the Cauchy stress tensor that is parallel to the pole of the fracture $\vec{n}$, and C_0 and μ_s are the cohesion and the friction of the fracture, respectively. In reality, the position, the orientation, the strength of fractures, and the stress conditions away from the wells are not accurately known in advance. All four of these parameters are highly uncertain away from the well and only probabilistic forecasts of their values are possible after studying their statistical distribution at the well.

Here, the pore-pressure distribution is considered to be an unobserved hidden state that can reactivate fractures, and a probability density function (PDF) $\mathbb{p}$ is defined for sequences of induced seismicity. The PDF is conditioned on the stimulation strategy, which controls the hidden state, as well as on field observations concerning the uncertain parameters. Besides the cumulative number of earthquake events and their moment magnitude, other important sampled characteristics of these sequences are the orientation of the reactivated fractures, the size and the direction of the slip, the stress drop of each earthquake, and how the permeability and the porosity are affected by each event. By combining deterministic modeling of flow and sampling of induced seismicity with $\mathbb{p}$, the space of possible sequences of induced seismicity is restricted into the subset of sequences for which the mass conservation is satisfied. The hybrid model here stochastically models the evolution of the cloud of induced seismicity events by sampling events at each moment with the PDF $\mathbb{p}$ conditioned on the pore-pressure solution of eq. (1). Such a run is called "forward run", henceforth. Opposite to the "forward run" stands the "inversion", during which the PDF $\mathbb{p}$ needs to be calibrated. Field observations, such as wellbore observations, seismic imaging, and the earthquake catalog collected during the stimulation, can assist in calibrating and making $\mathbb{p}$ less uniform.

2.3 Three dimensional discrete fracture hybrid model with HFR-Sim

The deterministic flow and heat transport modeling of the hybrid model described above is performed by the EGS simulator HFR-Sim, while the so-called "seed model" is employed for approximating the PDF $\mathbb{p}$. HFR-Sim employs the adaptive hierarchical fracture representation, which allows efficient discrete fracture modeling both in two-dimensional (2D) and three-dimensional (3D) scenarios with a dynamically changing fracture network (Karvounis and Jenny, 2016). When a size of a rupture area A_s is sampled by the "seed model" and this size is above a threshold value, then a discrete fracture is introduced into the fracture network that is modeled by HFR-Sim. When the ruptured area is less than the threshold value, HFR-Sim updates the hydraulic properties of an effective porous medium that is called "damaged matrix" and it captures the hydraulic effect both of structures with low permeability and of small fractures. The fracture network and the damaged matrix that result from a forward run with HFR-Sim, are also considered by HFR-Sim for the simulation of the production phase afterwards.

Usually, hybrid models are either lower dimensional or 3D continuum approaches that do not employ discrete modeling for important fractures. Discrete fracture modeling is essential for accurately capturing the thermal breakthrough curve in fractured reservoirs and accurately estimating E_{th} and t_l. Similarly, discrete fracture modeling can capture more accurately the propagation of pressure perturbations inside the reservoir, since it employs discrete representation for the highly permeable fractures, where the diffusivity of pore pressure is orders of magnitudes larger than in the rest of the reservoir. The adaptive hierarchical representation that is employed by the hybrid model can capture more realistically the pore-pressure breakthrough curve at the location of probable hypocenters and after many important ruptures have been modeled. Sampling of induced seismicity events with $\mathbb{p}$ in this hybrid model is conditioned to a more realistic pore-pressure estimation and hence its forecasting performance degenerates slower than in simpler hybrid models.

Last but not least, the discrete representation of fractures simplifies the calibration of the seed model, since a large portion of field observations can be processed and reproduced. For example, besides the measured hydraulic well logs and few statistics on the observed seismicity that can be processed from most hybrid models, the hybrid model discussed here can also include measurements obtained from seismic imaging, spinner logs, well images and focal planes, among others. Such observations usually cannot be processed by the rest of the hybrid models at all.

3. PROBABILISTIC FORECASTING

A Bayesian approach is employed for forecasting the outcome from different EGS operations, where M independent realizations of the seed model are simulated with HFR-Sim and M forecasts for the property U that is sought are obtained. Examples of U can be the

cumulative number of seeds that got reactivated in the seed model or the total thermal energy extracted. Mean values of U for the considered PDF $\mathbb{p}$ can also be approximated with a Monte Carlo integration such that

$$\langle U \rangle \approx \frac{1}{M} \sum_{k=1}^{M} U^k , \tag{7}$$

where U^k represents the k-th forecast, and the statistical error $\pm\delta U$ that is associated with the estimation $\langle U \rangle$ is equal to

$$\delta U \approx \sqrt{\frac{1}{M-1}\left(\frac{1}{M} \sum_{k=1}^{M} \left(U^k\right)^2 - \langle U \rangle^2 \right)} . \tag{8}$$

This way, different injection strategies F_{inj} can be compared to each other and with respect to the results of the Monte Carlo integration. A similar approach can be employed for finding an injection strategy that satisfies more than one objectives.

Performing a Monte Carlo integration with such a hybrid model comes at a price, since many computational resources are required and these resources should be optimally distributed. Large scale reservoir simulators typically employ parallel processing for accelerating the return time of their results, where the simulation is decomposed in smaller tasks that are executed in parallel by a large number of processors. Although such an approach can minimize the return time of a single simulation, it does not necessarily minimize the return time of a probabilistic forecast as in eq. (7). For example, if the size of the simulated scenarios required for an acceptable error δU is comparable to the number of available processors, then assigning one processor to each scenario will in theory lead to a faster forecast. Here, we consider Monte Carlo integrations with direct sampling, where the computational power is equally distributed to each simulation and each simulation requires exactly one processor.

3.1 Sampling Sequences of Induced Seismicity Events

Whenever a random number needs to be sampled from the hybrid model, then a number is read from a sequence with integers. This sequence of pseudorandom numbers has a large but finite size, and the elements of it are uniformly distributed inside a space that ranges from zero to the maximum integer value in the sequence. By dividing an element of this pseudorandom sequence with the size of the sequence's range, one can get a pseudorandom value that is uniformly distributed inside the space *[0,1)*.

In order to reliably approximate the expected value for the simulated property, it is important to sample each induced seismicity event independently and without bias. Thus, the hybrid model employs the 'sprng5' library, which can create scalable sequences of pseudorandom numbers (Mascagni and Srinivasan, 2000). Here, each simulation with the hybrid model is assigned its own unique sequence of pseudorandom numbers. Hence, repetition of similar sequences of random numbers occurs at a frequency that is consistent to the uniform distribution.

Here, we focus on sequences of induced seismicity that have constant stress drop, the slip along them is constant and isotropic, and the shape of the slipped area A_s is always a disc that is centered around the hypocenter. All hypocenters have the same friction and cohesion, and they are uniformly distributed inside Ω. A unit vector that is parallel to the pole of each sampled fracture $\vec{n}$ is sampled, which unit vectors are uniformly distributed inside the space $[0,4\pi]$. All Cauchy stress tensors have the same principal directions, but different values for their corresponding principal stresses. Each principal stress follows a normal distribution around a mean value and with a standard deviation that is proportional to this mean value. The Box-Mueller algorithm has been implemented for sampling pseudorandom numbers with a normal distribution, which algorithm returns two numbers that follow the random distribution method for every two numbers that are read from the uniform pseudorandom sequence. The statistical distribution of the moment magnitude inside the sequence of induced seismicity resembles to the Gutenberg-Richter law. The latter is achieved by assuming that the moment magnitude M_w of each event is sampled independently of the rest properties and according to the cumulative density function

$$F(M_w) = 1 - 10^{-b(M_w - M_{w,min})} , \tag{6}$$

where b is the b-value of the resulting Gutenberg-Richter distribution, and $M_{w,min}$ is the minimum possible moment magnitude. This b-value is considered constant both in space and time. A magnitude can be sampled, by sampling a real number inside *[0,1)* and then finding the value of M_w in eq. (6) that returns a cumulative density function equal to the sampled number. Due to the fact that the employed sequence of pseudorandom numbers is a discrete distribution and not a continuous one, more than one numbers from the sequence may be required for correctly sampling a large M_w. The sequence of pseudorandom numbers does not include values that are infinitely close to *1* and thus, when a value for M_w that is above a threshold value is sampled, sampling with eq. (6) needs to be repeated and this time the value $M_{w,min}$ needs to be equal with the latter threshold value for M_w. If this re-sampling is skipped and a very low value of $M_{w,min}$ is considered at the same time, then the final Gutenberg-Richter distribution would not be continuous away from $M_{w,min}$.

Overall, for each possible hypocenter at least 10 pseudorandom numbers are required. Only for the rare occasions where re-sampling with eq. (6) is required, more pseudorandom numbers are required. Since the number of possible hypocenters that need to be sampled with any seed model increases logarithmically with the $M_{w,min}$ considered, the size of the sequence of pseudorandom numbers that is employed is a limit to the number of possible hypocenters that can be sampled without the sequence being repeated during the same

forecast. Here, we consider problems in which the size of the sequence is sufficiently large to ensure that it does not bias the results of the MC integration.

3.2 Pore Pressure Diffusion

Equation (1), the solution of which is necessary to be deterministically approximated, is a parabolic partial differential equation and is solved implicitly; i.e. at each time step the unique change of pore-pressure that satisfies the discretized form of eq. (1) is found. This unique solution is found by solving a large sparse linear system, the solution of which requires a large portion of the overall computational resources. HFR-Sim employs the Algebraic MultiGrid (AMG) linear system solver from the Trilinos package to solve this system. In general, AMG algorithms demonstrate a linear relationship between the computational cost they require for solving a linear system and the size of the linear system, and the number of iterations that is required by an AMG algorithm until it converges to the solution of the next time step is rather independent of the size of the linear system. On the other side of implicit solutions stand the explicit solutions that require only one matrix-vector multiplication per simulated time step. The new time step's explicit solution for each cell is a linear combination of the previous time step's solution for a small set of cells (also called "stencil"). When fractures are explicitly discretized, explicit solutions are not feasible, since they can return stable solutions of overpressure only for tiny time steps and thus, the overall cost significantly exceeds the cost of an implicit solution with an AMG algorithm. Here, we present a variation of the adaptive implicit method (Thomas and Thurnau, 1983) that leads to smaller linear systems, it combines the advantages of the implicit and the explicit methods, and it is ideal for scenarios where the pore pressure is homogeneous initially.

Contrary to techniques that reduce the size of the linear system by re-meshing, such as the adaptive mesh refinement, the adaptive implicit method can operate in a single mesh and its solution consists of the implicit solution for a portion of the mesh and the explicit solution for the rest of the mesh. Important first step before proceeding to solving the linear system for a new time step is to separate the cells into three separate subsets. The first subset consists of all the matrix cells that have experienced up to that moment a pressure change larger than a threshold value, all the cells that either correspond to wells or discrete fractures, and all cells that correspond to a matrix and a well or a discrete fracture are embedded to it. The second subset consists of all matrix cells that have not yet experienced a pressure change larger than the threshold, but if an explicit method was to be employed for approximating their pore pressure, then at least one cell from the first subset would affect their explicit pore-pressure solution. The rest of the cells, whose explicit pore-pressure solution is not expected to be above the threshold value, are the third subset, their implicit solution is never updated, and no flux condition is assumed between them and the rest of the cells for this time step. Eventually, a linear system of significantly smaller size is solved by the AMG algorithm, the solution of which is in close agreement with the solution of the full linear system.

Important parameters for separating the cells are the threshold value for the changes of the pore-pressure and the stencil of the explicit solution. The separation of cells explained above can be implemented very efficiently in structured meshes like the one employed by HFR-Sim for the matrix. Initially, the first subset is updated and new cells that have to be included there are estimated. Then, the minimum number of stable explicit iterations that are required for the implicit time step is estimated, where time step restrictions due to fractures are neglected. Then, a graph search is performed for every new cell of the first subset and the rest of the subgroups are updated for the given stencil. The final linear system consists of the discretized equations for the cells from the first two subsets.

Here, the adaptive implicit method is implemented only when both the number of discrete fractures and the boundary conditions at the wells do not change. When this is not the case, then the implicit solution for the whole mesh is estimated. Last but not least, integration with an adaptive stepsize is implemented for the same time steps that the adaptive implicit method is employed. During these time steps, eq. (1) is assumed linear and hence the adaptive stepsize integration can be exploited. Practically, the solution's return times of the hybrid model are accelerated for periods without important seismicity. Long term simulations with the hybrid model can be concluded significantly faster.

4. EXEMPLARY SIMULATION OF TWO SINGLE REALIZATIONS

Here, the hybrid model that was presented in the previous sections is employed and a single realization of seeds is simulated with it for two different scenarios. In the first scenario, two wells that distance each other by approximately *0.42 km* are stimulated with exactly the same stimulation strategy, which is the flow rate injected during the stimulation of the EGS reservoir in Basel in 2006. In the second scenario, the same two wells are stimulated again, but this time the second well is not stimulated by injecting water through the whole open segment at once, but it is stimulated in four stages, where the open segment of the well is divided in four equidistant segments and the segments are stimulated one after the other. A period of 1 day is considered between changing segments and each segment is stimulated with the stimulation strategy from Basel normalized to the length of the segment, as plotted in Fig. 1.

The initial HFR-Sim model in both scenarios is such that it reproduces the well logs obtained from the well in Basel from the injection test that happened before the main stimulation. The initial permeability in the matrix is considered isotropic and equal to $2 \cdot 10^{-17}\ m^2$, the initial porosity is *1%* and the compressibility of the matrix is $7.2 \cdot 10^{-11}\ Pa^{-1}$. All fractures are allowed to reactivate only once during the stimulation, after their reactivation their mechanical aperture increases from *0.125 mm* to 1. *mm* and their hydraulic aperture becomes *0.2mm*. Their equivalent permeability is estimated with the cubic law for their hydraulic apperture and is approximately $3.33 \cdot 10^{-9}\ m^2$. The compressibility of all mechanical apertures is constant and equal to $1.8 \cdot 10^{-10}\ m/Pa$. The directions of the principal stresses and their principal values are close to the values estimated by Terakawa et al. (2012) for Basel after processing the obtained focal plane solution.

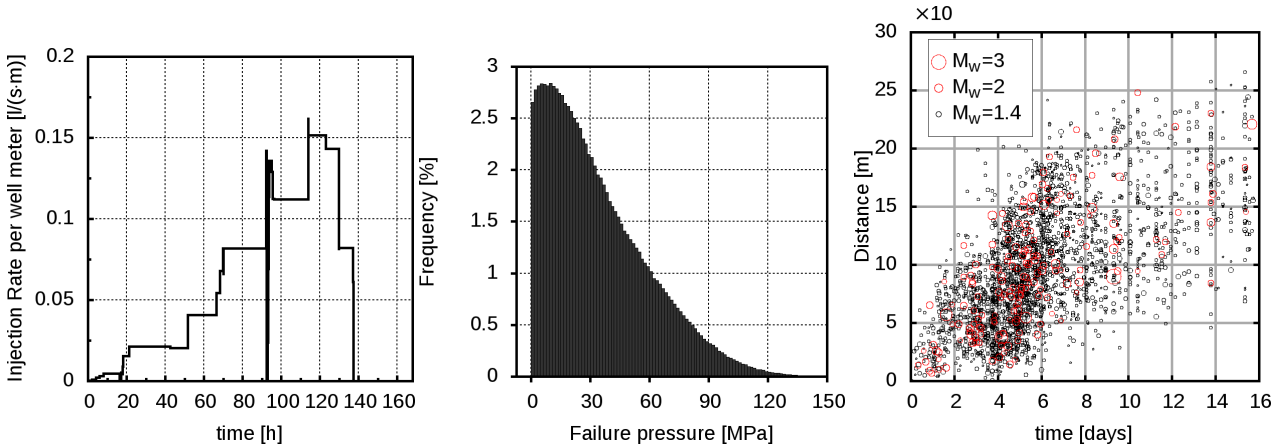

Figure 1: On the left, the stimulation strategy considered for all well segments . In the middle, a histogram of the failure pressure of the sampled seeds is plotted, which is an approximation of the probability density function for a seed's failure pressure. On the right, the source time, the moment magnitude M_w and the distance from the well of each simulated induced seismicity event during the stimulation of the first well are plotted.

Sampled seeds can have any orientation, are uniformly distributed in space with a density equal to *0.005 seeds/m*^{3}, and very critically stressed seeds that can trigger with pore-pressure changes less than *1 bar* are sampled. An approximation of the PDF for a seed to trigger at a certain pressure is plotted in Fig. 1. where the implemented stimulation strategy is plotted too. The minimum allowed moment magnitude sampled is set to $M_{w,min}$=*0.8* and the b-value with which M_w is sampled is *1.3*.

The simulation of the first well's stimulation, which is identical for the two scenarios, returns a cumulative number of approximately *1,391* induced seismicity events until the *16*th day, where the simulation stops. The distance of the modeled events from the well as well as their source time and moment magnitudes are plotted in Fig 1. For the second well, a total number of *1414* and of *1191* are simulated for the single and the four-stage scenarios, respectively. All the simulated events for the two scenarios are depicted in Fig. 2. As it is depicted there, the induced seismicity for the first scenario, where the well is stimulated at once, extended much further than in the scenario where the well is stimulated at four stages. The cloud of modeled seismicity from the first well is reached only in the 'single-stage' stimulation scenario and it is not reached when the second well is stimulated in 'four-stages'. This also partially explains why *15%* more events are modeled in the single-stage scenario than in the four-stage scenario.

The poor interconnectivity between the two wells in the scenario where the clouds from the two wells did not reach each other, is also confirmed when the production phase is simulated, where the same constant pressure difference of 60. MPa is assumed between the two wells, with which only 3.6 l/s of water are circulated between the wells, contrary to the scenario where both wells are simulated in a single stage and where 21.2 l/s are circulated. In both scenarios cold water of temperature 30°C is injected through the first well, hot water is produced through the production well, and no flux condition is assumed for the far field boundaries.

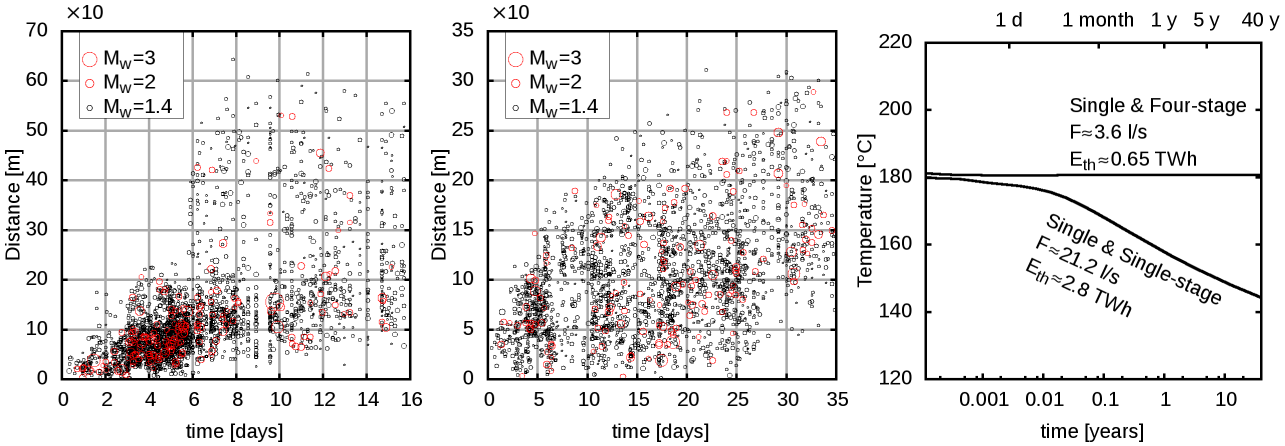

Figure 2: The source time, the moment magnitude Mw and distance from the second well of the simulated induced seismicity events are plotted for the stimulation of the second well in a single stage (left) and in four stages (middle). Events with Mw>2 have been colored as red. On the right, the time evolution of the temperature of the produced water is plotted for the two scenarios, when a constant pressure difference of *60 MPa* is considered between the wells.

The time evolution of the temperature of the produced water is plotted in Fig. 2 too. Although the temperature declines significantly faster in the scenario where both wells are stimulated at a single stage, overall significantly more thermal energy is extracted since larger rates of water are circulated. The total thermal energy extracted is *2779 GWh* and *649 GWh* for the first and the second scenario, respectively, which indicates how much more successful the single stage injection is for that particular set of seeds and for this stimulation strategy.

5. EXEMPLARY MONTE CARLO INTEGRATIONS

Here, the hybrid model is employed in exemplary MC integrations with *M=250* different realizations of seeds, where the mean cumulative number of modeled events is estimated. All computations are performed in the Euler high-performance computer at the CSCS data center in Lugano, Switzerland, thanks to which all MC integrations that are presented here were completed in approximately 4 hours. The injection strategy considered is again the injection strategy from the stimulation of the EGS reservoir in Basel (Fig. 1). Injection here happens in a single stage and for approximately the *5.4* first days. Then the following four scenarios are simulated:

A. stimulation continues for *6* more days during which period the pressure at the well head is kept steady at *30 MPa*.
B. the well shuts permanently,
C. fluid is pumped out of the well at a constant rate of *1. l/s*, and
D. fluid is pumped out of the well at a constant rate of *2. l/s*.

The same initial HFR-Sim model and the same aperture changes from each modeled event are considered, as in section 4. Here however, a less critically stressed set of seeds is considered, where very rarely an induced seismicity event is modeled for pore-pressure changes that are below *0.5 MPa*. The direction of the 2nd principal stress is considered vertical, and the other two directions of principal stresses are considered aligned to the maximum and the minimum horizontal stress as they were measured by Häring et al. (2008). The same values for the principal stress are considered for all seeds –independently of depth-, which are the values estimated by Häring et al. (2008) for a depth of *5. km*. The same b-value of *1.3* is considered here as before.

In Fig. 3 the mean value for the cumulative number of modeled events and its error are plotted for scenarios A and B. At the end of the 5.4th day, the expected number of events for these 250 scenarios, which is the same for all scenarios, is 306 ± 2.66 events with a moment magnitude above 0.8. If the well shuts permanently until the 90th day (scenario B), then the mean value reaches 477 ± 5 events, and 1681 ± 29.5 events if the pressure at the well is kept steady at *30 MPa* for 6 days before the permanent shutting of the well (scenario A). For scenarios C and D, where water is pumped out, the mean number of events at the 90th day reaches 464 ± 4.8 and 451 ± 4.4 events for 1 l/s and 2 l/s extraction rates, respectively. The mean curves of the latter two scenarios for the post-injection period are normalized with respect to the number of events that are expected during the post-injection period in scenario B. The normalized curves are plotted in Fig. 3 and can be compared. As one would expect, pumping out water reduces the total number of events and larger extraction rates lead to larger reductions of seismicity. When water is pumped out with *1. l/s*, more than *7%* of potential induced events are expected to be avoided and more than *15%* when the extraction rate is *2. l/s*. Note that, during the first days after the ending of injection, scenarios B-D have almost identical mean curves for their forecasted seismicity.

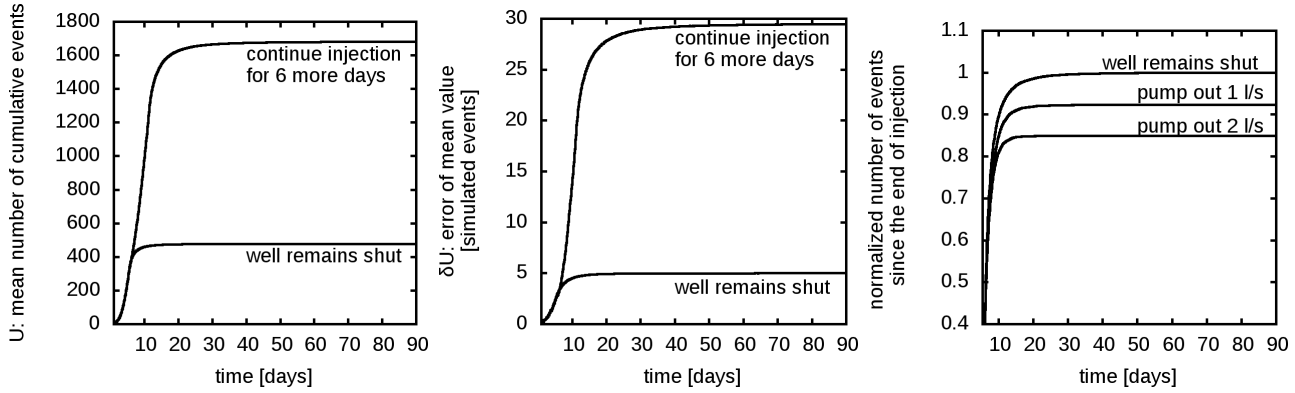

Figure 3: On the left, the time evolution of the mean cumulative number of modeled events is modeled for scenarios A and B and for *M=250* scenarios. The corresponding statistical errors of the MC integrations for scenarios A and B are plotted in the middle. On the right, the mean value of the cumulative number of events for scenarios B-D is normalized for the post-injection period, with scenario B as the reference curve.

6. CONCLUSION

Hybrid models combine deterministic flow modeling with stochastic geomechanical modeling, have shown abilities in forecasting characteristics of the induced seismicity, and are expected to play a crucial role in probabilistic assessments of induced seismicity hazard during the stimulation of future EGS reservoir in Switzerland. Here, the modeling approach of the hybrid model described by Karvounis and Wiemer (2015) is briefly explained. This hybrid model combines an EGS simulator with the geomechanical model, it considers more realistic numerical solutions for flow, and it can be employed for probabilistically assessing the efficacy of a stimulation strategy in complex EGS scenarios and for more than one target goals. One can perform with this hybrid model MC integration over the

space of uncertainty that characterizes both the geological model and the hypocenters inside it. Here, numerical issues that may lead to biased results during MC integration have been discussed, a description of how they have been treated by the hybrid model has been provided, and numerical recipes have been described, thanks to which the return time of an MC integration can be significantly reduced. Finally, the framework has been employed in two simulations, where the same geological model and the same set of probable hypocenters have been simulated with two different stimulation strategies, and in a number of exemplary MC integrations.

ACKNOWLEDGEMENTS

The authors appreciate the support of Geo-Energie Suisse in the development of the near real time traffic light.

REFERENCES

Catalli, F., Rinaldi, A. P., Gischig, V., Nespoli, M., & Wiemer, S.: The importance of earthquake interactions for injection-induced seismicity: Retrospective modeling of the Basel Enhanced Geothermal System. *Geophysical Research Letters*, 43(10), (2016), 4992–4999. https://doi.org/10.1002/2016GL068932

Gaucher, E., Schoenball, M., Heidbach, O., Zang, A., Fokker, P. A., van Wees, J.-D., & Kohl, T.: Induced seismicity in geothermal reservoirs: A review of forecasting approaches. *Renewable and Sustainable Energy Reviews*, 52, (2015), 1473–1490. https://doi.org/10.1016/j.rser.2015.08.026

Gischig, V., Wiemer, S., & Alcolea, A.: Balancing reservoir creation and seismic hazard in enhanced geothermal systems, *Geophys Journal International*, 198 (3): 1585-1598, (2014). https://doi.org/10.1093/gji/ggu221

Goertz-Allmann, B. P., Goertz, A., & Wiemer, S.: Stress drop variations of induced earthquakes at the Basel geothermal site. Geophysical Research Letters (Vol. 38), (2011). *American Geophysical Union*. https://doi.org/10.1029/2011GL047498

Häring, M. O., Schanz, U., Ladner, F., & Dyer, B. C.: Characterisation of the Basel 1 enhanced geothermal system. *Geothermics*, 37(5), (2008), 469–495. https://doi.org/10.1016/j.geothermics.2008.06.002

Karvounis, D., Gischig, V., & Wiemer, S.: EGS Probabilistic Seismic Hazard Assessment with 3-D Discrete Fracture Modeling. *Proceedings* of 39th Stanford Geothermal Workshop, (2014), 1–9.

Karvounis, D. C., & Jenny, P.: Adaptive Hierarchical Fracture Model for Enhanced Geothermal Systems. *Multiscale Modeling & Simulation*, 14(1), (2016), 207–231. https://doi.org/10.1137/140983987

Karvounis, D. C., & Wiemer, S.: Decision making software for forecasting induced seismicity and thermal energy revenues in enhanced geothermal systems. *Proceedings* World Geothermal Congress 2015, (April), 10. Retrieved from https://pangea.stanford.edu/ERE/db/WGC/papers/WGC/2015/31057.pdf

Király-Proag, E., Zechar, J. D., Gischig, V., Wiemer, S., Karvounis, D., & Doetsch, J.: Validating induced seismicity forecast models-Induced Seismicity Test Bench. *Journal of Geophysical Research: Solid Earth*, 121(8), (2016), 6009–6029. https://doi.org/10.1002/2016JB013236

Rinaldi, A. P., & Nespoli, M.: TOUGH2-seed: A coupled fluid flow and mechanical-stochastic approach to model injection-induced seismicity. *Computers & Geosciences*, in press., (2016). http://dx.doi.org/10.1016/j.cageo.2016.12.003

Mascagni, M., & Srinivasan, A.: Algorithm 806: SPRNG: a scalable library for pseudorandom number generation. *ACM Transactions on Mathematical Software*, 26(3), (2000), 436–461. https://doi.org/10.1145/358407.358427

Terakawa, T., Miller, S. A., & Deichmann, N.: High fluid pressure and triggered earthquakes in the enhanced geothermal system in Basel, Switzerland. *Journal of Geophysical Research*, 117(B7), B07305, (2012). https://doi.org/10.1029/2011JB008980

Thomas, G. W., & Thurnau, D. H.: Reservoir Simulation Using an Adaptive Implicit Method. *Society of Petroleum Engineers* Journal, 23(5), (1983), 759–768. https://doi.org/10.2118/10120-PA

Trutnevyte, E., & Wiemer, S.: Tailor-made risk governance for induced seismicity of geothermal energy projects: An application to Switzerland. *Geothermics*, 65, (2017), 295–312. https://doi.org/10.1016/j.geothermics.2016.10.006